5.1 Introduction

Reduced graphene oxide (rGO) is two dimensional layered structure of graphene. Applications of this material can be summarized (K.I. Bolotin,et al.2008; A.K. Geim,et al.2007; X.S. Li,et al.2009; C. Lee,et al. 2009; A. Pruna,2016; Y. Zhao,et al. 2017) as super-capacitors, fuel cells, electrochemical detection of inorganic and organic electro-active compounds and photoactive devices. Reduced graphene (rGO) possesses exciting properties (H. Lu,et al. 2014; G. Ni, et al.2012; W. Jie,et al. 2014; A. Kafy, et al.2015; R. K. Jammula,et al.2015; B. Wen, et al.2014) such as high mobility and conductivity, high optical transparency, mechanical flexibility, chemical stability and high specific surface area. The structure of reduced graphene (rGO) possesses a single layer of sp^2 carbon atom and two-dimensional honeycomb lattice structure (K. S. Novoselov,et al. 2005).The oxide form of graphene, connected to oxygen functional groups viz. carboxylic acid groups (-COOH), hydroxyl groups (-OH) and an epoxy group (-C-O-C) on both edges and hybridized surface of the basal plane through sp^3 hybridization.The variation of carbon to oxygen ratio of graphene oxide affects the band gap ranging from semi-metal to semiconductor (Y. Zhang,et al.2005; B.Y.Zhu, et al.2010; G. Eda, et al.2009; S.M. Jilani,et al. 2012;Y.Yang, R. Lulu, et al.2011).

The optical, electrical, and mechanical properties of rGO can be altered by combining it with other materials like metals and semiconductors (Z.Wan, et al. 2012; B. Li, et al.2012). GO-based nano-composites with ZnO, TiO_2 have high

electron mobility and also suitable photocatalytic applications (P.V. Kamat2010; M.H. Huang,et al.2010).The ZnO is a promising semiconductor having anenergy band gap of 3.37 eV which has a strong luminescence at room temperature. It has been suggested by Kamat et al. (P.V. Kamat 2010), that embedded ZnO can enhance the optical and electrical properties of rGO nanocomposites through the carboxylic functional groups. However, the morphology of ZnO has been considered in recent research activities to obtain structures such as nanorods, nanowires, nanobelts, and nanotubes. These types of structures influence the properties and their device applications (Z.L.Wang, 2004; M. Law,et al.2005; D.C. Look2001). For optical and semiconducting devices, ZnO is a better semiconductor material and it can be referred as an n-type transparent semiconductor material with a wide direct bandgap and a large exciton binding energy.Its stability upon exposure to high energy radiation makes it superior to the other materials (S. Naseem, et al.1993). Above mentioned properties make ZnO a desirable material for many optoelectronic applications (K. Kanasuqi, et al. 2009, P. Kathirvel, et al.2014).

Keeping the above-mentioned facts, the recent literature reveals that a particular structure such as tube or rod shapes ZnO could be utilized in making composites with rGO. Taking this idea in the present research work, columnar structures ZnO was prepared and it was further embedded in GO by reduction process to obtain nanocomposite hybrid system.There are different processing routes for synthesis of ZnO nanoparticles with certain morphology such as sol-gel method (A.E. Danks,et al. 2016), hydrothermal method (J. Dinget al.2015), assisted solution route (M. Darwishet al.2016), two-step method (B. Bhushanet al.2017), aqueous

chemical route (M. R. Parra., F.Z. Haque, et al. 2014) and chemical precipitation method (Q. Yang, et al. 2010).Among them we have applied a two-step method as discussed in the section of materials and methods for the synthesis of the columnar morphology of ZnO in a hybrid system of reduced graphene oxide composites.

This method comprises lower complexity, inexpensive, a higher degree of purity and more possibility to obtain columnar structure compared to the other synthesis method. These composites were utilized for photocatalytic application and results revealed that composite materials had a good photocatalytic performance with natural dye under sunlight irradiation.

5.2 Results and Discussion

5.2.1. Structure and Morphological properties of ZnO columnar structures

The GO was prepared by modified Hummers method (W.S.Hummers 1958). The synthesis method of rGO has been discussed in chapter-3 (section-**3.4.1).** The sample of graphite and reduced graphene oxide (GO) were coded by GR and GO respectively. The columnar morphology of ZnO with GO, synthesized by two step method at different pH. The synthesis method of rGO-ZnO has been discussed in chapter-3 (section-**3.4.3)**. The samples were coded as RZ-pH6, RZ-pH9, RZ-pH12 respectively. Here RZ is denoted to reduced graphene oxide and zinc composites. The structural characterizations of the samples were carried out by XRD. The XRD patterns of graphite (GR), GO and RZ composites at different pH are shown in figure 5.1(a). A very strong peak at angle 26.76° of the plane (002) in RG curve shows a typical pattern of the graphitic crystal structure with d-spacing of 0.335A°. The intensities of the GO peaks were very low as compared to graphite as observed in the

insert portion in figure5.1 (b). No other peaks were observed, which indicates the removal of functional groups. The d-spacing of GO is 0.73nm which is larger than the d-spacing (0.335nm) of GR. This is the indication of removal of the oxygen-containing group on carbon nanosheets. The XRD patterns of RZ composites prepared at different pH values are showing the variations in results, confirming its influences on the crystallinity of the materials. In RZ composites, ZnO peaks with their millar indexed planes are represented by peak marked as 'Θ' and additional peaks are marked as 'Δ' and 'σ'. Reflection planes of the 'Θ' peaks for the sample RZ-pH6, RZ-pH9 and RZ-pH12 have been mached with the standard JCPDS card no 36-1451 (shown in appendix-2) and listed in appendix-9, 10 &11. Reflection planes of the 'Δ' peaks have been mached with the standard JCPDS card no 41-1487 (shown in appendix-1) and listed in appendix-4&5. The 'Δ' peaks are similar to that of carbon black (T.V. Cuong, et al.2010), and indicates the restacking of the reduced graphene sheets (H.L.F. Eduardo,et al. 2007; H.P. Cong et al.2010). Reflection planes of the 'σ' peaks have been mached with the standard JCPDS card no 25-1029 (shown in appendix-3) and listed in appendix-16&17. The 'σ' peaks indicate that the GO is not completely reduced and hence it can be concluded that the chemical reduction always results in the presence of few defected zinc oxalate ($C_2H_2O_4Zn$) like impurities. The appearance of these peaks was decreased with increasing pH. The RZ-pH6 sample exhibited a very intense and sharp feature as compared with the XRD pattern of RZ-pH9 and RZ-pH12. This shows that the crystallinity is decreasing with increase in the pH value of RZ composites science in RZ-pH6 the acidic nature dominates which restrain hydrolysis while in RZ-pH9 and RZ-pH12 the alkali nature accelerates the hydrolysis present in the solution (M.J. Chithra, et

al.2015). It can be concluded here that ZnO embedded in GO converts it to rGO and decrease in pH improves the crystalline structure of the prepared composite samples. The major plane (101) of RZ-pH6 is significantly present, while other are seen with comparatively lower intensities. Estimation of ZnO crystalline size in RZ composites was done using equation (3.7) and lattice constant was calculated using equation (3.9).

The lattice constants and estimated error bars (±σ) of measured lattice constants, "a" and "c" for all samples are listed in table 5.1. The crystalline size for all samples is also listed in table 5.1. The calculated lattice constants are in good agreement with JCPDS card 36-1451(table 5.1). From the data listed in table 5.1, it was found that the lattice constant and crystallite size changes in different composites due to the presence of rGO (D.Fu, G.Hanet, al.2012).

The figure.1 (b) shows that the crystalline peak of RZ-pH9 and RZ-pH12 are shifted when compared with RZ-pH6. This indicates the variation of lattice parameters because of the presence of carbonaceous materials. From the data listed in table 5.1, it is also found that the average crystallite size of RZ-pH6 and RZ-pH9 are 43nm and 13nm respectively which shows that the lattice constant is also affected by the pH value of the samples. This variation of crystal size and lattice constant is due to alkali medium of RZ composite. These are also confirmed by variation of dislocation density as given in table 5.1. Thus pH value and carbonaceous material present in RZ composite play a vital role in the material crystal size. From the table 5.1 the cell voume of the sample RZ70, RZ80 and RZ90 are varying with increasing

the pH. It is minimum for RZ-pH12 than RZ-pH6 and RZ-pH9 due to variation of the lattice contant with increasing the pH (B. Rajesh Kumar, et al.2017).

The lattice strain and stress are believed to have a great influence on the physical properties of nanomaterial. XRD profile analysis is a well-executed technique for estimating the microstrain. From the available models, the Williamson-Hall (W-H) method is the most simplified and extensively studied technique (V. Mote et al.2012) for analyzing the crystallite size and lattice strain.

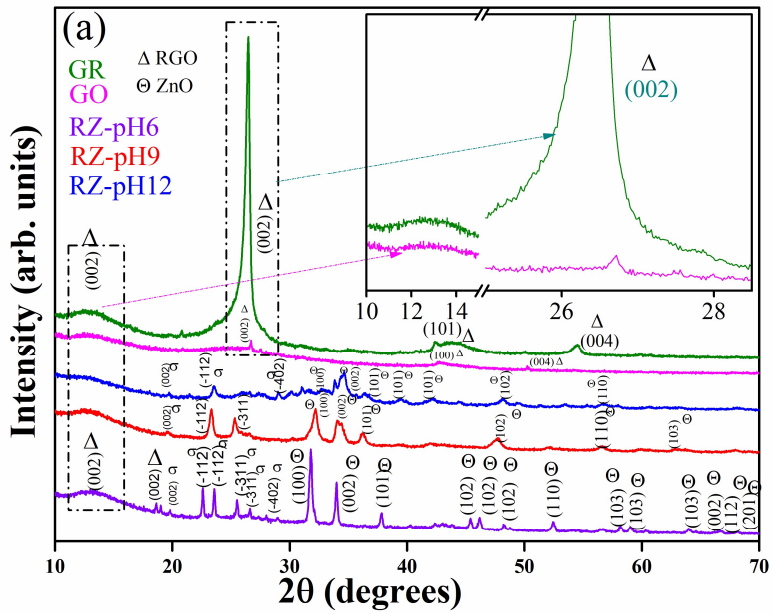

Figure 5.1(a) XRD patterns of graphite (GR), Graphene oxide (GO), RZ-pH6, RZ-Ph9 and RZ-pH12.

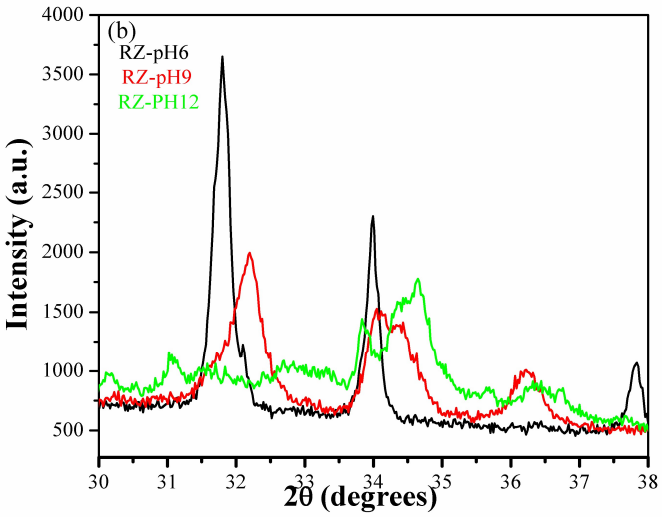

Figure 5.1 (b) Corresponding XRD peak shift of RZ-pH6, RZ-pH9 and RZ- pH12

W-H analysis is an integrated method, in which the crystallite size and strain-induced line broadening of the XRD profile can be calculated from the peak width using mentioned equation in chapter-3 (equation-3.23 and 3.24) for W-H model (J. Pelleg,et al.2005). From the linear plot of $\beta_{hkl}\cos\theta$ vs $4\sin\theta$, we can calculate the strain as well as the size of the crystallite. In principle, the slope of the graph gives the strain, whereas the reciprocal of the intercept should be the crystallite size (P. Bindu2014). Figure 5.1(c) represents the W-H plot of RZ-pH6 and RZ-pH9 of composite powder respectively. A positive strain of RZ-pH6 and RZ-pH9 around the value 2.64498 x 10^{-4} and at 5.18x10^{-4} was observed from the slope of figure 5.1(c) respectively. The crystallite size calculated from the intercept of RZ-pH6 and RZ-pH9 were 41nm and 14nm respectively, which is also approximately similar to value as calculated by equation 3.7.

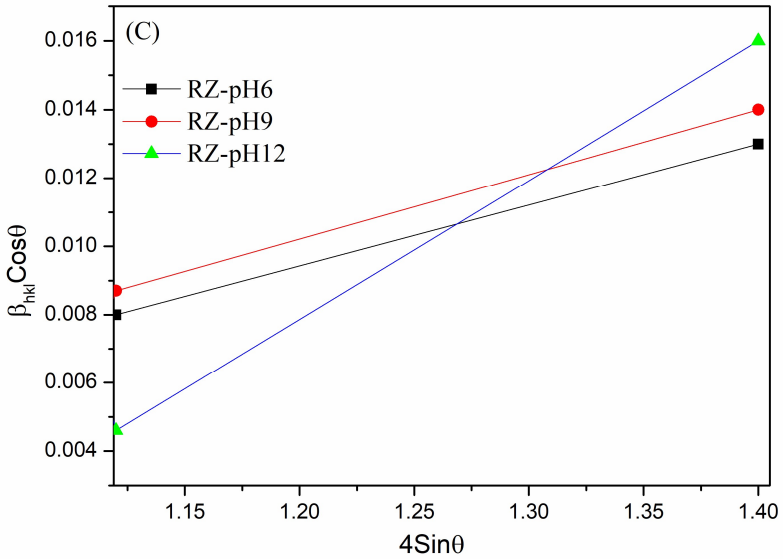

Figure 5.1 (c) Williamson-Hall analysis of RZ-pH6, RZ-Ph9 and RZ-pH12.

Table 5.1 The physical properties of the columnar structure of ZnO in RZ composites prepared in this work.

Sample	Unit cell parameters		Cell volume(A^0)^3	Crystalline size(nm)	Micro strain (line/m^2) (1x10-^{4})	E_g (eV)
	a± σ [A^0]	**a**/c ± σ [A^0]				
RZ-pH6	3.291 ±0.041	1.597 ±0.005	49.29	43	$4x10^{-4}$	3.2
RZ-pH9	3.271 ±0.003	1.598 ±0.005	48.43	13	$8x10^{-4}$	3.25
RZ-pH12	3.247 ±0.003	1.602 ±0.0001	47.49	10	$4x10^{-3}$	3.3
Card	3.250	1.6021				

The crystal size calculated by plane (101), a and c are lattice parameters calculated on the bases of plan (100) and (002), the energy band gap E_g is obtained based on the absorption spectroscopy.

The surface morphologies of RZ-pH6, RZ-pH9, RZ-pH12 and GO powder were investigated by scanning electron microscopy (SEM) and are shown in figure 5.2(a–e). The figure 5.2 (a-b) displays SEM with EDX of RZ-pH6 which shows the formation of the columnar morphology of ZnO. The EDX analysis shows that only C, O and Zn signal have been detected which indicates the absence of impurity. It

has been reported that the presence of carbonaceous material changes the lattice constants of ZnO (D. Fu, et al.2012). Similarly, in our sample, it is seen that the increase in GO concentration from 0.01wt% to 0.05wt. %, the agglomeration of the particles occurs. Another effect for the growth of ZnO in columnar shapes is its reaction in acidic medium because in the chemical reaction when $ZnSO_4.7H_2O$ reacts with NaOH, it produces Zn $(OH)_2$. This further hydrolyzed in $[Zn(OH)_4]^{2-}$ and it acts as a growth unit (D. Sharma et al.2011). The concentrated NaOH solution produces Na^+ in composite solution which may intercalate ZnO growth unit. Due to their large surface-to-volume ratio and high surface energy.This ZnO morphology grows spontaneously from curled shapes to the columnar shape of ZnO structure.

The average diameter of columnar shape measured with the help of scaling of SEM, were obtained in the ranging 0.8-1.57µm to 0.42-0.84 µm respectively. The increase in pH from acidic to the alkaline, columnar shape of ZnO agglomerated to each other as shown in figure5.2(c). The SEM image of the sample RZ-pH12 in figure 5.2 (d) shows the shape of ZnO in a distorted manner, and it may be due to the NaOH. It has been observed that the structures are dependent on pH in all the SEM images which suggested that the pH value affected the ZnO structure of the samples in a hybrid system of RZ composite and also altered the order of crystallinity. These results showed that the acidic medium is suitable for the development of the columnar shape of ZnO. In figure 5.2 (e); crumpling of GO sheets appeared, indicating the dehydration of sheets (M. Xiaofeiet al.2012).

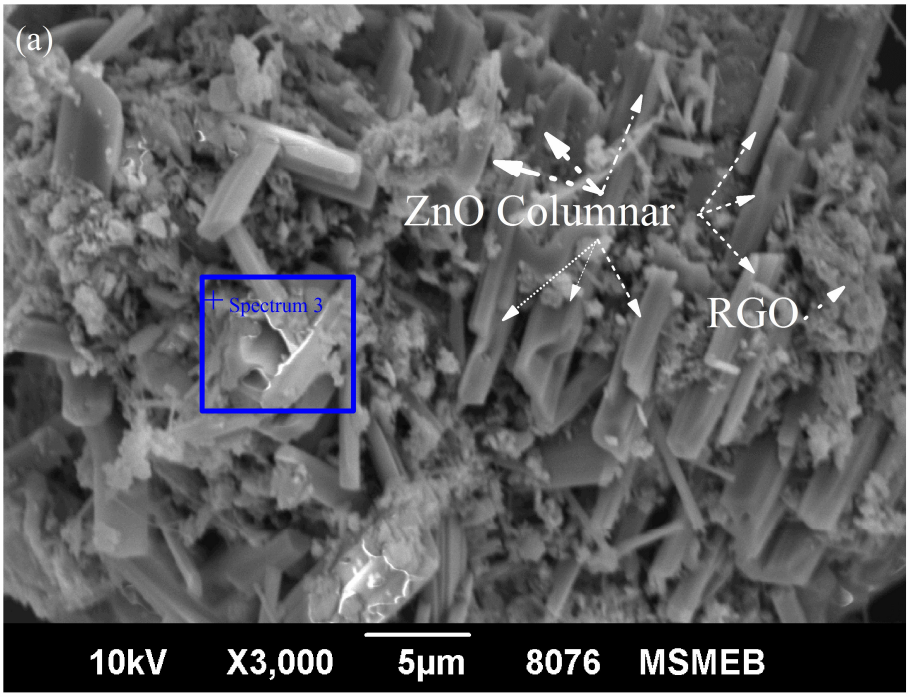
(a)
ZnO Columnar
RGO
Spectrum 3
10kV X3,000 5µm 8076 MSMEB

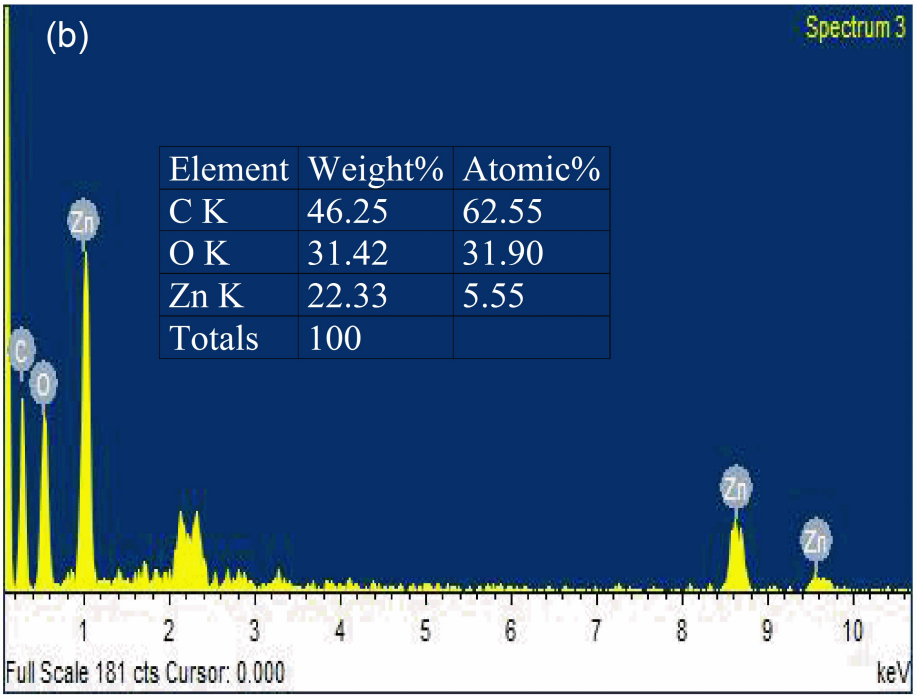
(b)
Spectrum 3
Element Weight% Atomic%
C K 46.25 62.55
O K 31.42 31.90
Zn K 22.33 5.55
Totals 100
Zn
C
O
Zn
Zn
1 2 3 4 5 6 7 8 9 10
Full Scale 181 cts Cursor: 0.000
keV

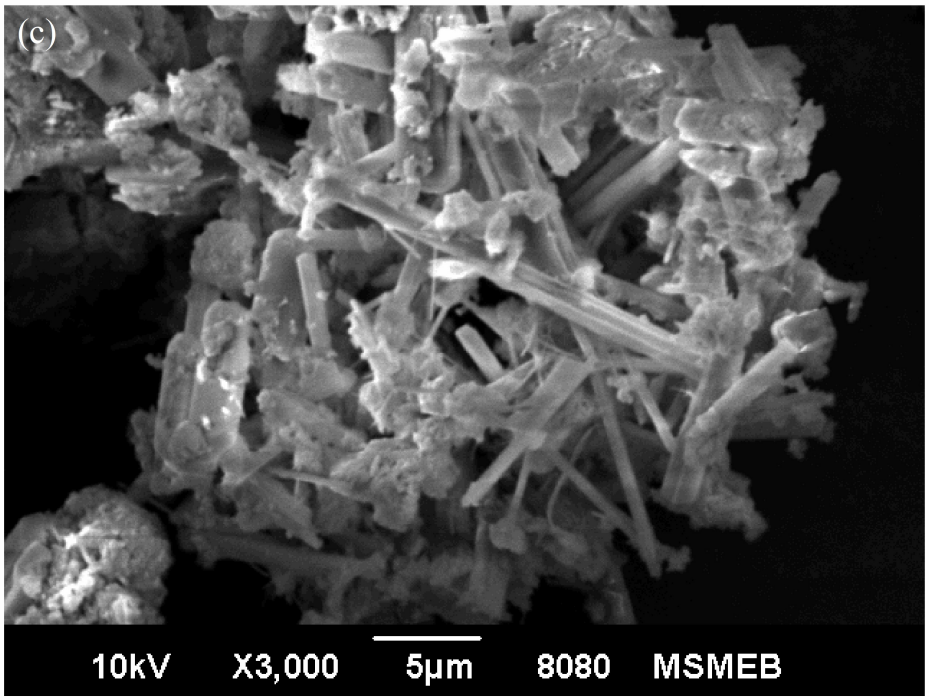
(c)
10kV X3,000 5µm 8080 MSMEB

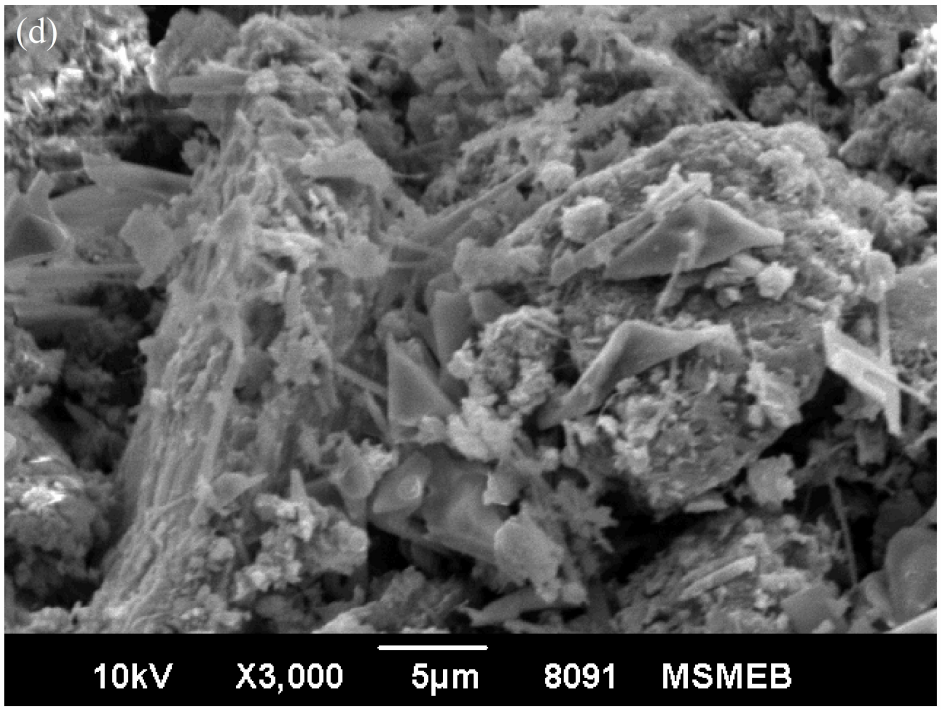
(d)
10kV X3,000 5µm 8091 MSMEB

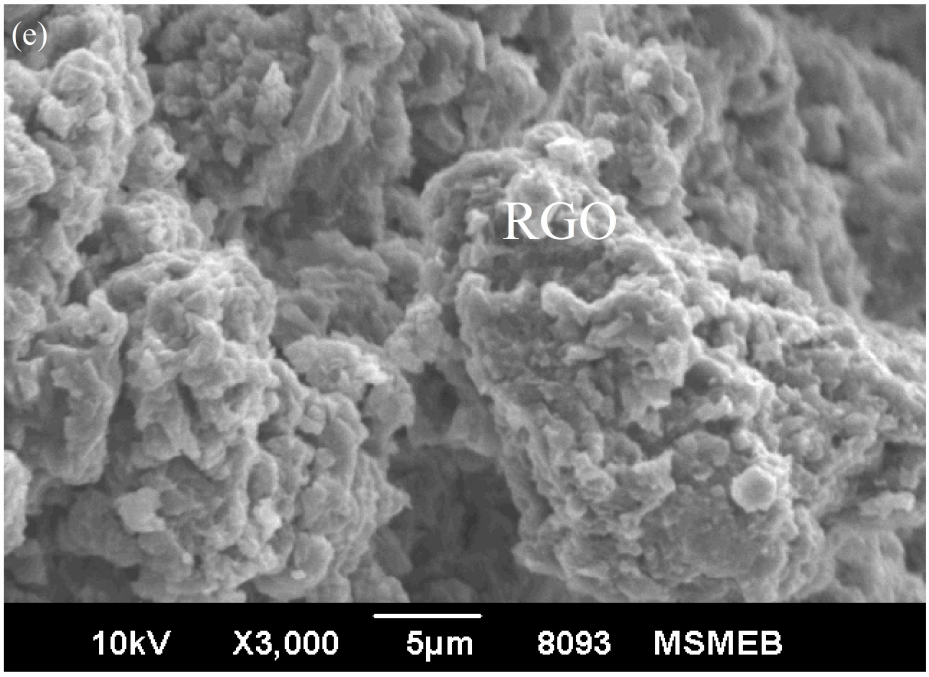

Figure 5.2 (a) SEM Image of RZ-pH6, (b) EDX Image of RZ-pH6, (c) SEM Image of RZ-pH (d) SEM Images of RZ-pH12 (e) SEM Image of reduced graphene oxide.

Figure 5.3[(a)-(d)] shows the HR-TEM image of RZ-pH9. The dark sections represent ZnO and appear as rod-like; belt-like which is shown in figure 5.3 (a). In figure 5.3 (b) shows pencil-like, in figure 5.3 (c) shows hammer and palm-like, in figure 5.3 (d) shows the tendency of the overlapping of two rods and forming a T like shape. All the different type ZnO structures have a dimension in nanoscale. So sample RZ-pH9 have a different shape of ZnO morphology due to agglomeration of ZnO nanoparticles with increasing the pH value. Because in acidic medium the solution concentration of H^+ ions is increased, this may be favorable condition for the growth of columnar morphology of ZnO in RZ composite solution. In alkaline medium, the concentration OH^- ions are increased which may be favorable to the agglomerate or overlap the growth of ZnO nanoparticles and form a different shape

of ZnO. It is observed the distribution of different structure morphology of ZnO over the rGO sheets will improve the charge separation which will increase the photocatalytic activity. In the SAED pattern, preferred orientations are along the plane (100) and (002). In our work, we perform the photocatalytic activity using the catalytic RZ-pH6 because having the particular morphology as likes columnar.

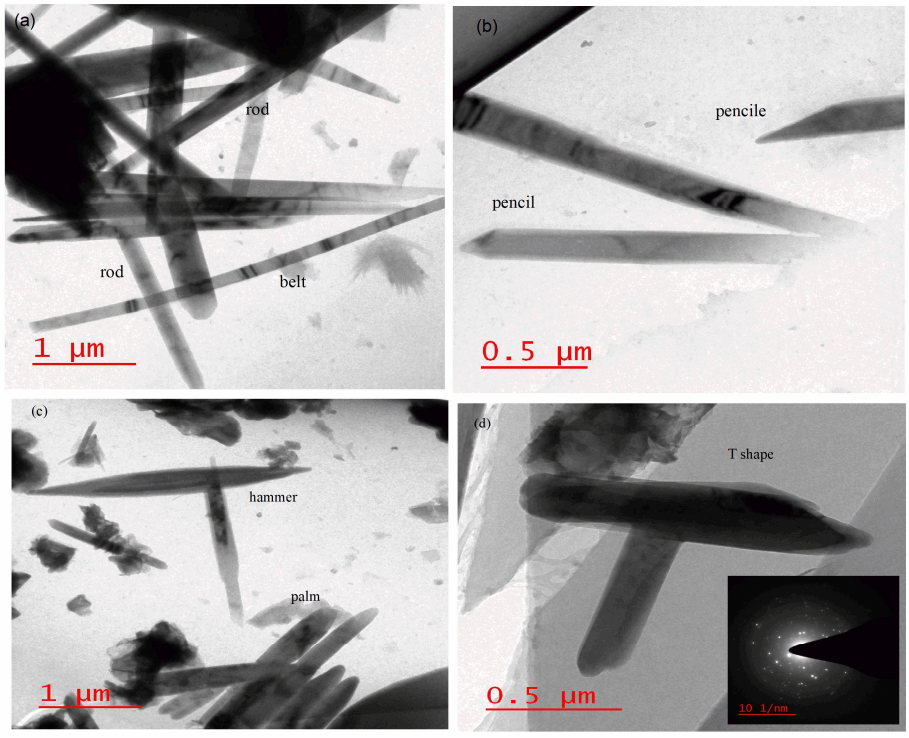

Figure 5. 3 HR-TEM images of RZ-pH9 with labeled by (a) rod and belt like, (b) Pencil like, (c) hammer and palm like, (d) T-shape like, in inset was the SAED pattern of ZnO.

FTIR analysis of RZ-pH6, RZ-pH9, and RZ-pH12 composite samples are shown in figure 5.4.The band at 3428 cm^{-1} signifies the hydroxyl groups of absorbed H_2O molecules. It is observed that peaks width of sample RZ-pH6 decrease with increasing the pH value from acidic to alkaline medium and become the narrow peak of the sample RZ-pH12 as compare to the RZ-pH6 and RZ-pH9 because the

additional amount of O-H from drop-by-drop adding NaOH in composite solution react with the $ZnSO_4.7H_2O$ to the pH values ≥6. The strong asymmetric stretching mode of variation of C= O was observed between 1628cm^{-1}-1562cm^{-1}. It is also observed that the peak C= O was shifted which indicates the variation of structure morphology. The peak C-OH (1172cm^{-1}) and C-O (1126cm^{-1}) are observed in the composites. Other groups such as carboxylic group at 1410cm^{-1}and hydroxide group at 1250cm^{-1} disappeared in this spectrum. The standard broad peak at 450 cm^{-1}is analogous to pure ZnO, and it is vibrating in stretching modes (N. Lepot, al.2007). It is also observed that stretching vibration of ZnO in range 450cm^{-1}-450cm^{-1} is decreased with increasing pH value. This change indicates the changes in morphology of ZnO analogous to SEM and TEM results. Stretching mode in sample RZ-pH6, RZ-pH9, RZ-pH12 are similar. This pattern indicated the shifting peaks dramatically, and some of them disappeared after the reduction treatment, showing the absence of most of the functional groups that comprised of oxygen in the GO.

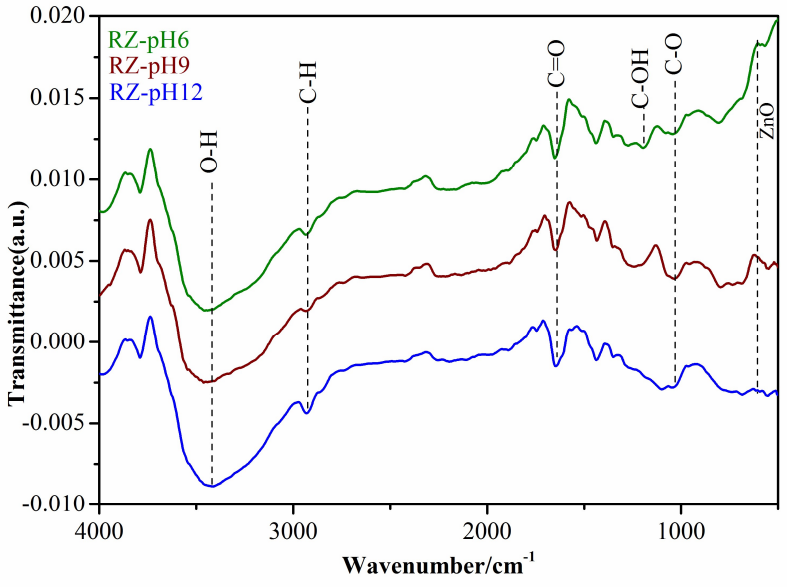

Figure 5.4 FTIR spectra of RZ-pH6, RZ-pH9 and RZ-pH12.

5.3 Evaluation of optical and photocatalytic properties

5.3.1 Uv-visible Absorption spectroscopy

UV-visible normalized absorption spectraof RZ-pH6, RZ-pH9, and RZ-pH12 are shown in figure 5.5. The sharp characteristic of absorption peak signifies the crystalline structure and impurity present in ZnO structures. The absorbance of RZ composite depended on pH value when changes from 6 to 9. On further increase in pH value, the absorbance dropped down. RGO contains in the composites increased the absorbance in the visible region (X. Liu Zhaoet, al.2012). The optical band gap of the RZ composites at different pH value was determined by extrapolating the linear region of the $\alpha h\upsilon^2$ versus energy plot as shown in the insert of figure 5.5(b). The insert of figure 5.5 (b) shows the band gap values of RZ-pH6, RZ-pH6, and RZ-pH9 about 3.2eV, 3.25eV and 3.3eV respectively and listed in table 5.1. From this table the crystallite size of RZ-pH12 is smaller than RZ-pH6 and RZ-pH9. In this regard, according to quantum confinement theory, the enery band gap of semiconductor depends on the crystal size; its value will increase with a decrease in crystal size. Hence the enery band gap of RZ-pH12 is increased than RZ-pH6 and RZ-pH9 due to quantum confinement effect. The variation in band gap was due to the morphology of ZnO and wt% of GO in RZ composites. Therefore, the presence of RGO in ZnO and obtained columnar morphology of ZnO were beneficial to increase the intensity of light absorption and for enhancement in the photocatalytic activity performance (T.G. Xu, L.W. Zhang, et al.2011).

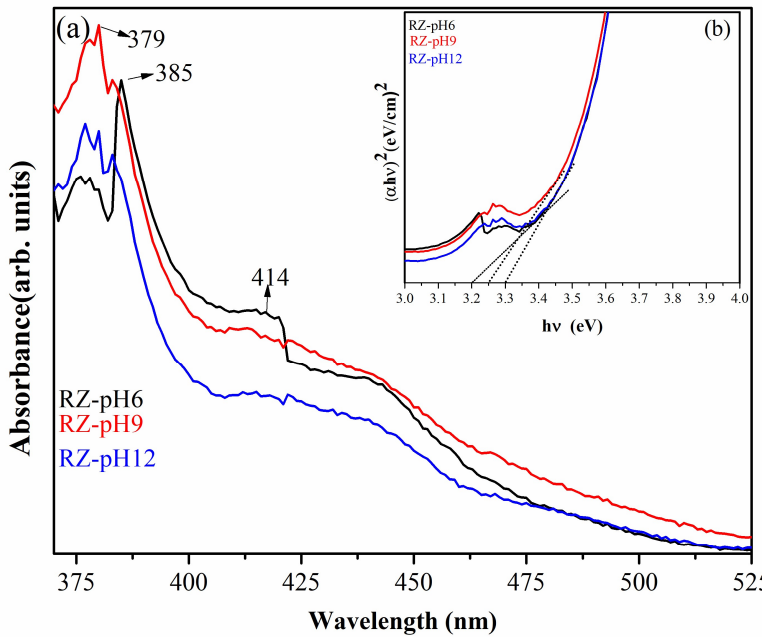

Figure 5.5 UV-visible normalized absorption spectra of RZ-pH6, RZ-pH9 and RZ-pH12.

The Ramanspectroscopy of RZ-pH6, RZ-pH9, and RZ-pH12 are shown in figure 5.6.There are two prominent peaks at 1350cm^{-1}(D band) and 1580cm^{-1}(G band) corresponding to the breathing mode of K-point phonons of A_{1g} symmetry and the E_{2g} phonon of sp^2 carbon atoms respectably (S.Park, A. Jinho et al.2009). The D' peak in RZ-pH9 at 1604 cm^{-1} were obtained in our sample. The peak D and D' are defect induced peak and the intensity ratio of the D to G band (I_D/I_G), as shown in figure 5.6 is a measure of the degree of graphitization and proportional to the average size of the sp^2 domains in the samples. This ratio increased from 0.83 to 0.84 indicating the degree of reduction (A.C. Ferrari et al.2006). The higher intensity of the D band in prepared RZ composites reflected more defect than inGO associated with grain boundaries/vacancies (F. Tuinstra, et al. 1970;R. Schonfelder, et al.2007) and amorphous carbon(S. Stankovich,et al. 2007). The other Raman mode obtained at 2624cm^{-1}(2D'-mode) in RZ-pH6 and at 2644 cm^{-1} in RZ-pH12. The 2D peak was

slightly shifted as compared to the RZ-pH6 and disappeared in RZ-pH9. The G peak also shifted as compared to the RZ-pH6 and RZ-pH12.This indicated that RZ composite is reduced.

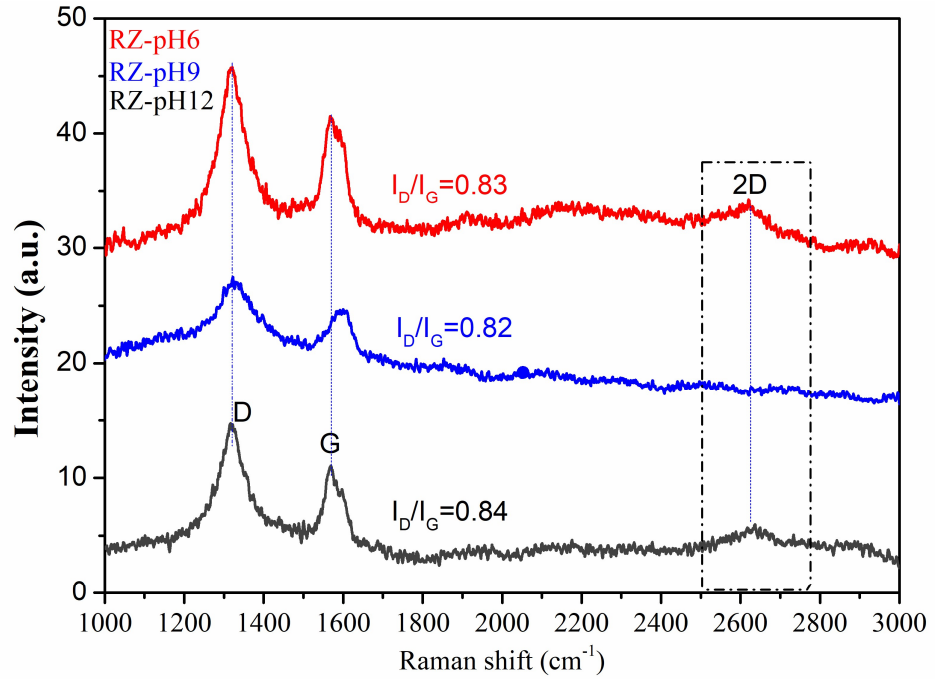

Figure 5.6 Raman spectrums of RZ-pH6, RZ-pH9 and RZ-pH12.

5.3.2 Photocatalytic degradation activities of RZ-pH6 with ND

For photocatalytic activity measurement of natural dye, was performed by the leaves of peepal tree known as Ficusreligiosa. Its extraction of chlorophyll is discussed in chapter-3(section **3.5.2)**. Here extracted chlorophyll is called nature dye and denoted as ND. The UV-visible spectrum of ND, RZ-pH6 with ND, its image and their optical band gap obtained by extrapolating the linear region of the $\alpha h\upsilon^2$ versus energy plot shown in figure 5.7 (a). There were no absorption peaks in UV range of pure ND, and only appeared in the visible region at 664nm. In the case of RZ-pH6 with ND,maximum absorption peaks appeared in the UV-visible region at

217nm for rGO, 325nm for ZnO and 664nm for ND. In the insert in figure 5.7 (a) shows the band gap values of RZ-pH6 and ND, found in the range of 3.0-5.9eV.This variation in band gap was due to the RGO, ZnO and ND concentration in composites solution. The photocatalytic activity was performed in the photocatalytic experiment shown in figure 5.7 (b) [(also discussed in figure 3.7 (b)] and recorded with UV-visible spectrum. The UV-visible spectrum of RZ-pH6 with ND and its image with increasing irradiation time between 0-120min over the surface of a photocatalytic shown in figure 5.7 (c). The maximum absorption peaks of each sample occurred at 664nm in the visible region. It can be seen that with an increased exposure time of sunlight, the absorbance of RZ-pH6 with ND was continuously decreasing but did not decreased under the dark condition and exhibited better photocatalytic performance. The absorption of light, transportation of charge and separation during photocatalytic were key factors when RGO was introduced into ZnO (H.Zhanget al.2010).The addition of RGO in the composite of ZnO increased the absorption intensity of visible light of the ZnO having a columnar morphology and there was a decrease pattern in the recombination of an electron-hole pair, resulting in enhanced photocatalytic performance. The reusability of RZ-pH6 for three successive cycles of adsorption and desorption of ND was determined in ethanol as shown in figure5.7 (d). It could be seen that the recycled use of RZ-pH6 for three times which influenced photocatalytic activity and indicating that it can be reused for the adsorption of organic pollutants. It is also important to specify here that the particles size of RZ-pH6 in micron range having columnar morphology which is easily separated from the solution and could be further reused. However, the concentration of RZ-pH6 for the first cycle decreased with increasing irradiation time, and it further

slightly decreases for the second and third cycles. This is due to the photo-corrosion effect of ZnO (H. Zhang et al.2010). Figure 5.7(e) shows a percentage degradation curve for the catalysts RZ-pH6. It is observed that the degradation efficiency of ND with RZ-pH6 is 64.40% achieved in 120 min which is calculated by the Eq (3.5).

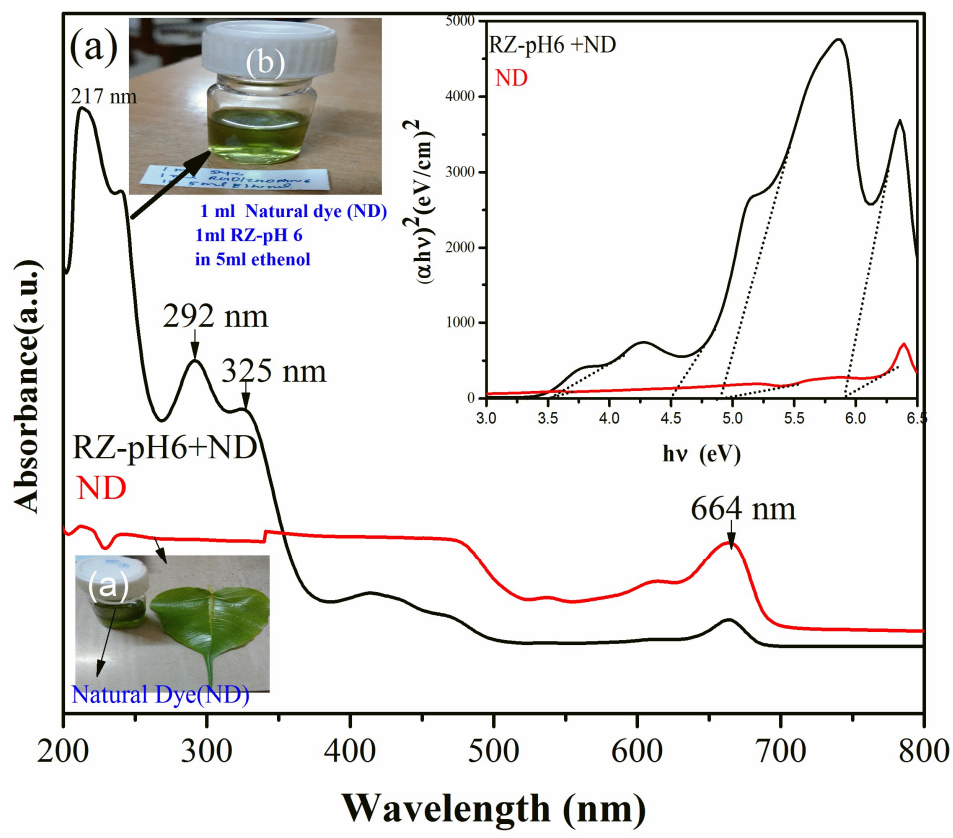

Figure 5.7 (a) UV-Vis Spectrum of ND and RZ-pH6 with ND solution and Insert of Plot of $(\alpha h\nu)^2$ vs. photon energy $h\nu$ for ND and RZ-pH6 with ND solution.

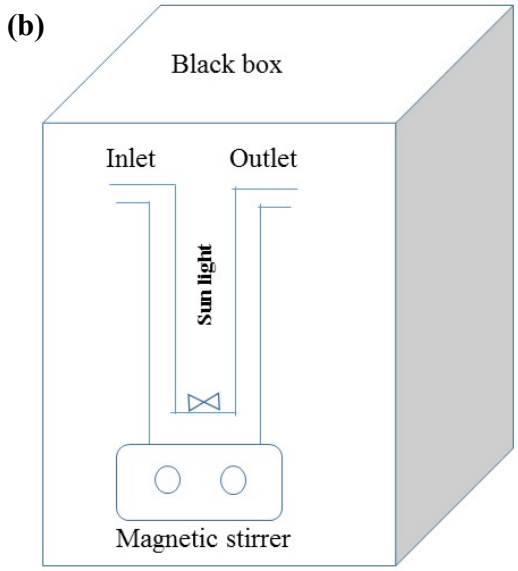

Figure 5.7 (b) Shachamatic diagram of photocatalytic experiment.

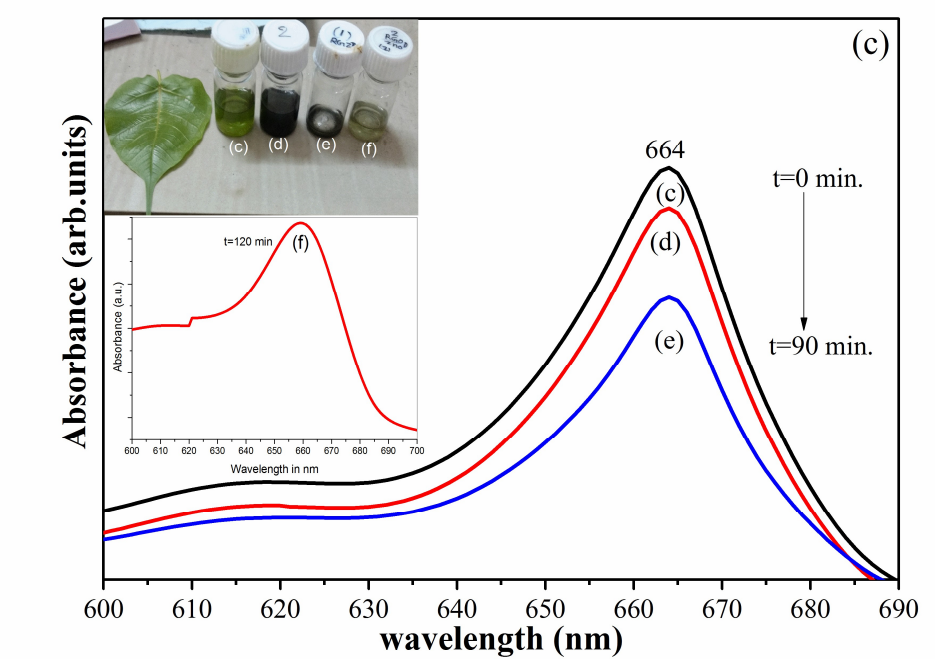

Figure 5.7(c) Time-dependent absorption spectra of ND solution with RZ-pH6 photocatalytic.

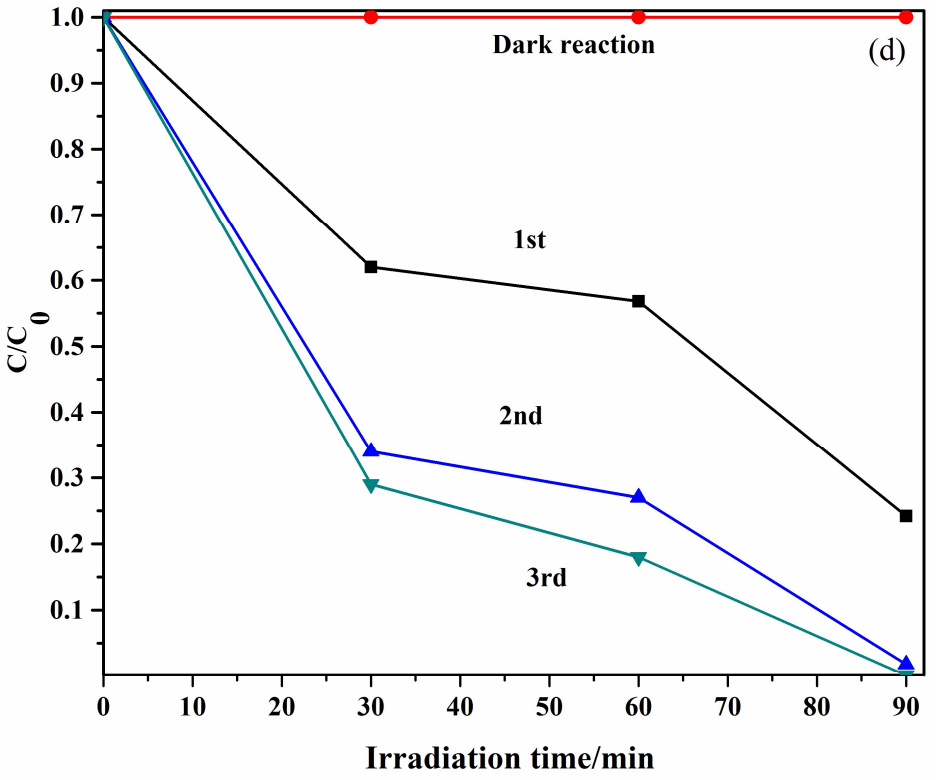

Figure 5.7(d) Photo-stability of ND solution with RZ-pH6 by three times of cycling uses.

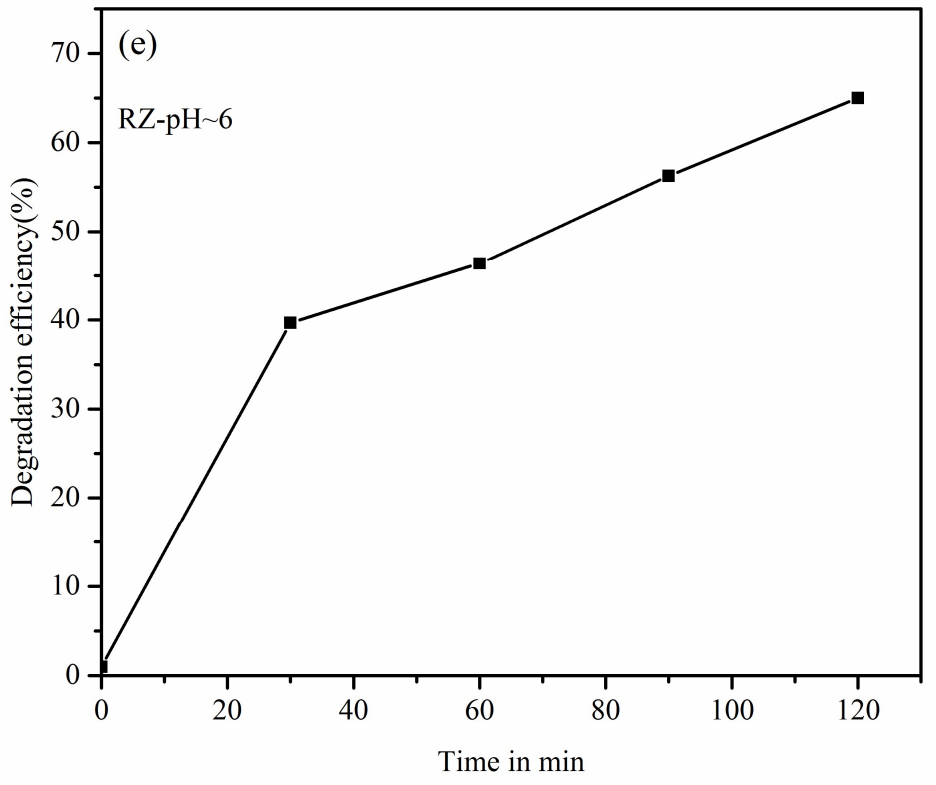

Figure 5.7(e) Photocatalytic degradation efficiency of ND solution with catalyst RZ-pH6.

5.5 Kinetics of degradation

Photocatalytic degradation kinetics for ND solution is analyzed with the RZ-pH6 catalyst which shown in figure 5.7 (f). The kinetic study was carried out at 1mlND solution and catalyst loading of 0.01mg/ml. For the low catalyst concentration, Langmuir-Hinshelwood first-order kinetic reaction is followed (T. Lv, L. K. Pan et al.2011) and expressed as

$$In(C_0 / C) = kt. \quad \text{---------- (5.1)}$$

Where$k$ is the degradation reaction rate constant in min^{-1} C_0 is the initial

concentration, t the reaction time and C_t the concentration at time‘t’. The plot of $In(C_0 / C)$ against ‘t’ is a straight line with slope k which is determined via linear regression. The concentration (C/C_0) varied during the photocatalytic experiment and depended on the maximum absorbance (A/A_0). The major reaction steps in this photocatalytic mechanism under sunlight irradiation are summarized by the following equation.

$$ZnO + h\nu \xrightarrow{sunlight} ZnO\ (e^- + h^+) \text{ ---------- (5. 2)}$$

$$ZnO\ (e^-) + RGO \rightarrow ZnO + RGO\ (e^-) \text{ ---------- (5.3)}$$

$$ZnO(h^+) + OH^- \rightarrow ZnO + .OH \text{ ---------- (5.4)}$$

$$.OH + N\ D \rightarrow \text{ degradation product ---------- (5.5)}$$

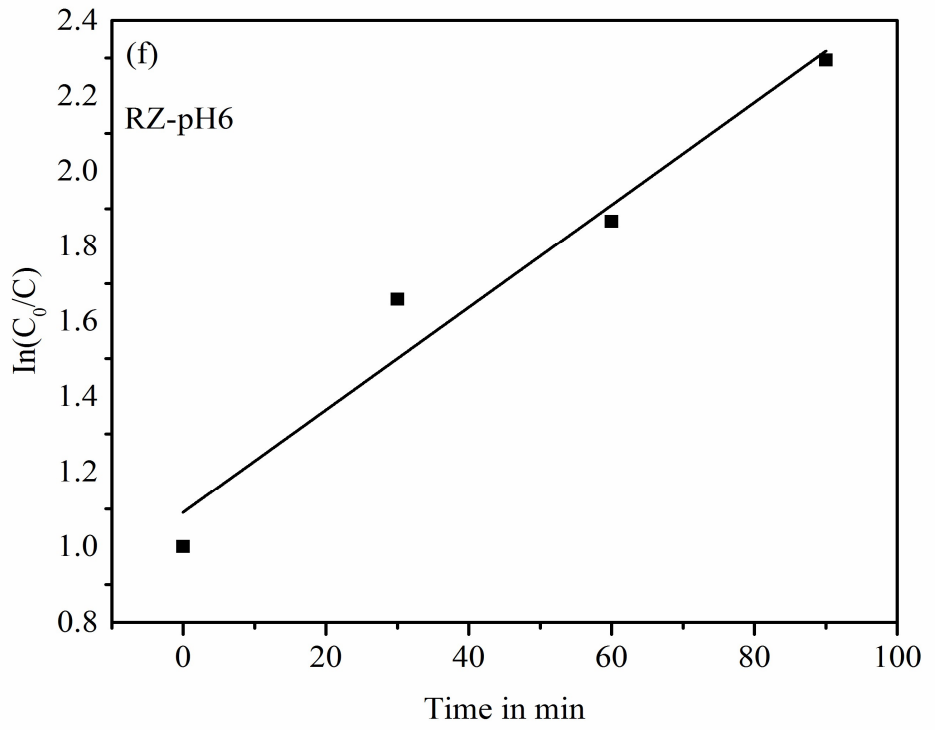

Figure 5. 7(f) Kinetic plot of of ND solution with catalyst RZ-pH6.

Figure 5.8 shows the enhanced photocatalytic activity due to the narrow band gap of RZ. There was an adjustment in energy levels among the ND, RGO, and ZnO by charge transfer when there was an induced visible light absorption in ND. The absorption of ND molecules was also affected by the surface area of RGO. The electrons from the excited ND could be easily transferred to the rGO after sunlight illumination because of the conductive nature of rGO and its work function level (Y. Gon, C. Zou, et al.2014). It may be beneficial for electron transfer from CB of ZnO to graphene layer. The RZ composite served much well as photocatalyst on degrading ND than the pure ZnO (Khokhra, R., Singh, R.K., et al.2015, Tang, Y.B., Lee, C.S. et al.2010). While rGO absorbed the ND on its surface by p-p stacking and affected the photodegradation process. This can be concluded that the rGO did not directly involve in the photodegradation process as a reaction agent. As shown in figure5.8, the electronic interaction between ZnO and RGO was one the crucial factor for the efficiency of separation of generated charges. The photocatalytic activity performance of different morphology of ZnO with RGO-ZnO nanocomposite in previous reported in the literature and our present morphology is listed comparatively in Table 5.2. In our work, although the columnar shape of ZnO structure samples with RGO was irradiated sunlight with lower catalyst loading (RZ-pH6), achieved degradation efficiency was increased with increasing exposure time under sunlight.

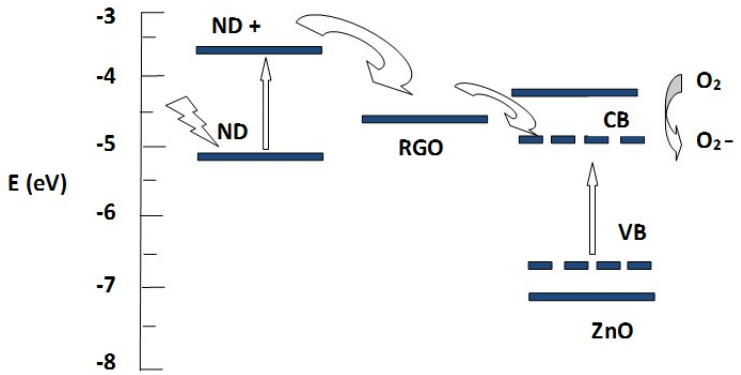

Figure 5.8 Photocatalytic degradation process of ND by the RZ-pH6 composite under visible light illumination. Electrons from ND + (excited state of ND) flow to the conduction band (CB) of ZnO through the RGO. Dotted lines represent the intra band gap energy levels ZnO, which were narrowed by the interaction between ZnO and RGO during the synthesis of the RZ composites.

Table 5.2 Comparative study of degradation efficiency of RGO-ZnO based photocatalysts.

Phocatalysts	Experimental condition			Degradation efficiency (%)	Ref.
	Catalyst loading ($mg\text{-}L^{-1}$)	Dye	Light source:	Irradiation times	
rGO –ZnO	30	Methylene blue	Xe lamp200W	50min 80%	R.Schonfelder,et al.2007
rGO –ZnOpH~11 (nanoparticles and nanorods)	20	Methylene blue	UV lamp 12W	120 min	T.V.Cuong, et al.2010
rGO –ZnO(sphere)	0.2	Methylene blue	Visible irrad.	90min	H.Zhang, et al.2010
rGO –ZnO nanowire	20	Rhodamine 6G	Mercury lamp 150W	30minT.Lv, et al.2011	
RGO-ZnOpH~6 Colomar shape	0.01	Natural Dye(ND)	Sunlight	120 min 64.40%	Present study

5.6 Summary of results

A simple powder processing method has been successfully demonstrated for preparation of columnar-shaped ZnO structures with an average diameter ranging 0.8-1.57μm. The analysis of XRD, SEM, HR-TEM, and Raman spectroscopy results indicated that the RZ composite structures can be easily synthesized with improved crystallinity and higher degrees of reduction in the prepared samples could be obtained. The UV–visa and Raman spectroscopy results also showed that graphene oxide in the RZ composites is in reduced form. The obtained properties of the composites with present method confirmed that the materials morphology have influenced the absorption and photocatalytic activity of natural dye under sunlight irradiation and result in maximum degradation efficiency 64.40% achieved in 120min and degradation efficiency increase with the increase in exposure time under sunlight.